# Forward Modeling of Ceres' Gravity Field for Planetary Protection Assessment

Yu Takahashi[1], Dan Grebow[1], Brian Kennedy[1], Julie Castillo-Rogez[2]
*Jet Propulsion Laboratory/California Insitute of Technology, Pasadena, CA, 91109, USA*

*and*

Nicolas Rambaux[3]
*IMCCE, Observatoire de Paris – PSL Research University, Sorbonne Universités – UPMC Univ. Paris 06, Univ. Lille 1, CNRS, 77 Avenue Denfert-Rochereau, 75014 Paris, France*

**The Dawn spacecraft arrived at the dwarf planet Ceres in early 2015 after a two and a half-year cruise in deep space after departing Vesta. The nominal plan for Dawn included successively lower science orbits, the last of which is called the Low Altitude Mapping Orbit that also serves as the disposal orbit after the end of mission. Prior to Dawn's arrival at Ceres, it was identified that Dawn would have to meet planetary protection requirements at Ceres by remaining on a stable orbit for 20 years past the end of the mission. With little a priori knowledge on Ceres' interior we analyzed what gravitational perturbations influence the long-term dynamical evolution of Dawn around Ceres and validated that the gravitational model of Ceres with the then-current best estimate of the density distribution model does not exceed the permissible bounds. The forward modeling of gravity fields from various shape models and density distribution was deemed valid to satisfy the planetary protection guidelines. This analysis was further confirmed after a new shape model based on the actual optical images was created. The gravity field as measured in the High Altitude Mapping Orbit also fits within the bounds of gravitational field studied pre-arrival at Ceres to substantiate our methodology used to satisfy the planetary protection requirement.**

## Nomenclature

| | | |
|---|---|---|
| $U$ | = | Gravitational Potential |
| $G$ | = | Gravitational Constant |
| $M^*$ | = | Reference mass (nominally the total mass of the body) |
| $R^*$ | = | Reference radius |
| $r$ | = | Spacecraft position |
| $P_{nm}$ | = | Associated Legendre function of degree $n$ and order $m$ |
| $C_{nm}$, $S_{nm}$ | = | Spherical harmonics of degree $n$ and order $m$ |
| $T_{nm}$, $U_{nm}$ | = | Topography of degree $n$ and order $m$ |
| $J_n$ | = | $-C_{n0}$ defined for convenience |
| $\lambda$ | = | Longitude of the spacecraft in the body-frame |
| $\phi$ | = | Latitude of the spacecraft in the body-frame |
| $N_{nm}$ | = | Normalization factor for spherical harmonics |
| $\kappa_n$ | = | Kaula rule of degree $n$ |

[1] Member of Mission Design and Navigation Section, Jet Propulsion Laboratory 4800 Oak Grove Drive, Pasadena, CA, 91109.
[2] Research Scientist in the Planetary Science Section, Jet Propulsion Laboratory 4800 Oak Grove Drive, Pasadena, CA, 91109.
[3] Associate Professor, IMCCE Institut de Mécanique Céleste et Calcul des Ephémérides, 77 Avenue Denfert-Rochereau, 75014 Paris, France.

## I. Introduction

The Dawn spacecraft arrived at dwarf planet Ceres in early 2015 after completing observation of Vesta in 2012. Vesta is the second most massive object in the main asteroid belt, and Dawn finished its science campaign in 2012 (Ref. 1). Ceres is the most massive object in the main asteroid belt between Mars and Jupiter and became the first dwarf planet to be orbited by a man-made object. Utilizing its ion propulsion system, Dawn became the first spacecraft to orbit two extraterrestrial bodies in the solar system. After a two and a half year cruise, the capture by the Ceres' gravitational field, where the orbital energy of the spacecraft becomes negative relative to the central body, occurred in March 2015. Refinements of the final plans for the Ceres mission occurred during the deep space cruise prior to the Approach. From the Rotational Characterization and onward, the Dawn spacecraft was inserted into four distinct polar orbits at successively lower altitudes. The nominal mission consisted of Approach, Rotational Characterization (RC3), Survey, High Altitude Mapping Orbit (HAMO), and Low Altitude Mapping Orbit (LAMO) phases. The final, lowest orbit called LAMO is an orbit with an average altitude of 350 km. Due to the failure of two of the four reaction wheels prior to Ceres arrival and limited hydrazine used for attitude control purposes, the nominal plan is to acquire as much science as possible by combining the two remaining wheels and the reaction control system for attitude control before consuming all the hydrazine. Once the hydrazine was fully expended, the spacecraft would remain at LAMO altitude. This final disposal orbit is subject to the guidelines set forth by the Planetary Protection (PP). Its purpose is to avoid contamination of celestial body by hardware that has not been sterilized prior to launch. Although the Dawn mission science targets (i.e., Vesta and Ceres) are in category II, the Mars flyby component of the mission makes Dawn a category III PP mission (Ref. 2). The PP guidelines supplied to the Dawn Project by the NASA Planetary Protection Office stipulated that the project must provide a spacecraft orbital lifetime around Ceres of greater than 20 years post orbit insertion, based on the worst-case credible gravity field.

This manuscript discusses how the Dawn navigation team approached this planetary protection requirement prior to the arrival at Ceres. The analysis was done at a time where the observations of Ceres were limited to the ground-based and space-based (i.e., Hubble Space Telescope) telescopes and thus the gravity field of Ceres was largely unknown. This uncertainty dominates the evolutional path taken by Dawn's orbit around Ceres. This study demanded a statistical approach involving Monte Carlo (MC) analysis of Ceres' gravity field as well as the long-term dynamical propagation of Dawn spacecraft under those gravity fields. We will first look at the dynamical sensitivity of the spherical harmonics to the long-term orbit propagation.

## II. Nominal Ceres Gravity Field and its Sensitivity to Orbit Stability

The gravitational potential of a celestial body is expressed by Equation 1:

$$U = \frac{GM^*}{R^*} \sum_{n=0}^{\infty} \sum_{m=0}^{n} \left(\frac{R^*}{r}\right)^{n+1} P_{nm}(\sin\phi) \begin{bmatrix} \cos(m\lambda) \\ \sin(m\lambda) \end{bmatrix} \cdot \begin{bmatrix} C_{nm} \\ S_{nm} \end{bmatrix} \tag{1}$$

This gravitational potential is expressed in the body frame since it is a function of the density distribution. The gradient of the gravitational potential with respect to the spacecraft position yields the gravitational acceleration. The reference radius is 476.9038 km for the rest of the paper. The body-fixed frame is computed from the best estimate from images obtained with the Hubble space telescope prior to Dawn's arrival at Ceres (Ref. 3). Because the navigation software at JPL, MONTE, implements normalized spherical harmonics, all values and uncertainties associated with them in this manuscript are for the normalized coefficients. The normalization is expressed as:

$$N_{nm} = \sqrt{(2-\delta_{0,m})(2n+1)\frac{(n-m)!}{(n+m)!}} \tag{2}$$

where the unnormalized coefficient is divided by $N_{nm}$ to yield the normalized coefficient. For the rest of the paper all cofficients are assumed normalized unless stated otherwise.

The first task we embarked on was to analyze the sensitivity of each spherical harmonic coefficient to the long-term propagation of the Dawn spacecraft dynamics. The forces acting on the spacecraft are the gravitational field of

degree and order six and solar radiation pressure. There are no maneuvers after the end of the mission. Table 1 shows the gravity field that was used for this orbital propagation study:

Table 1: Preliminary parameters for initial long-term orbit stability study.

| | Nominal | 1-sigma |
|---|---|---|
| GM ($km^3/s^2$) | 63.13 | 0.0135 |
| $J_2$ | 0.00940 | 0.0016 |
| $J_3$ | 0 | 0.0209 |
| $J_4$ | -0.000316 | 0.0075 |
| $J_5$ | 0 | 0.0005 |
| $J_6$ | 0.0000305 | 0.00015 |

The monopole (GM) of Ceres in Table 1 was obtained from Ref. 4. The uncertainty in GM is not of particular concern for the long-term perturbation, because it does not change the relative strengths of the harmonic terms. We are more interested in the interplay between the harmonic terms and how each coefficient can actually depart from the nominal values once Ceres' gravity field becomes known. To gauge the sensitivity of each harmonic term, we varied the each coefficient from the nominal value and applied the Monte Carlo perturbation study on the Dawn trajectory. The uncertainties for the parameters in this study were obtained from the covariances provided for maneuver design architecture studies for anticipated injection into the initial science orbit (RC3) around Ceres. We used the uncertainties from the initial orbit because initallly we believed they reflected our worst-case knowledge of the gravity field. A total of 1,000 samples were run with the same initial condition in LAMO for 20 years. The spherical harmonics are drawn from a normal distribution.

With the amount of data we collected, it is challenging to find a clear-cut metric characterizing a good (remains in orbit) or a bad (crashes into the body) trajectory. One metric that showed a distinct signature between the good and bad trajectories is the relative strength of $J_3$ and $J_4$ coefficients as shown in the scatter plot of Figure 1.

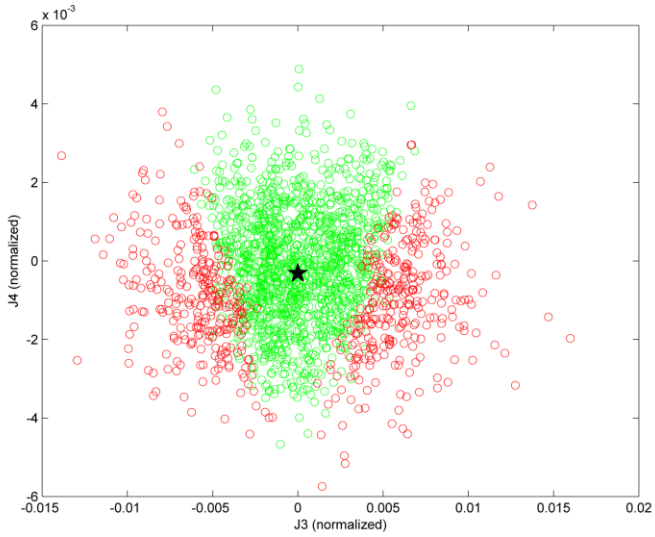


**Figure 1: Scatter plot of LAMO orbits that impact (red) vs orbits that propogate safely (green).** *Each point is shown as a function of of $J_3$ and $J_4$ obtained from Monte Carlo analysis. The star shows the mean nominal values for Ceres' gravitational coefficients.*

It was apparent from this preliminary study that non-impacting trajectories were strongly correlated to $J_2$, $J_3$, and $J_4$. The transition from trajectories that impact Ceres and those that do not are observed in Figure 1. In general large values of $J_3$ increase the eccentricity of the LAMO orbit, and, if sufficiently large, result in impacts. If $J_4$ is negative and sufficiently large in magnitude, impacts also result. We also noticed that the boundary between impacting and non-impacting trajectories in Figure 1 is sensitive to $J_2$ which has a stabilizing effect on the orbit. In order to better understand the relationship between $J_2$, $J_3$, and $J_4$ and their effects on long duration propagations, the team explored

the effect of varying the low degree zonal harmonics with a grid search. For each pair of $J_3$ and $J_4$ values, a sample LAMO orbit was propagated 50 years, well beyond the 20 year requirement stipulated by the Planetary Protection. The grid search was repeated for various values of $J_2$ to realize how the boundary line separating impact and non-impacting trajectories is influenced by $J_2$. These effects may be observed in Figure 2.

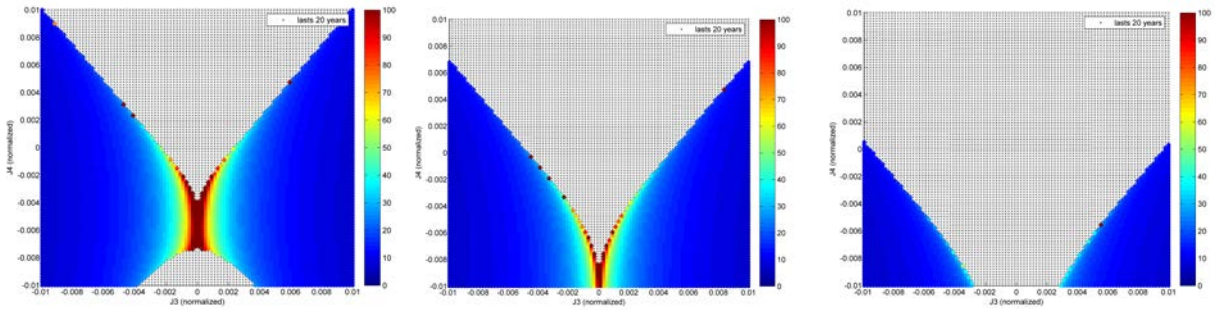


**Figure 2. Grid Search of $J_3$ and $J_4$ for three different values of $J_2$ showing evolution of boundary between impacting and non-impacting trajectories, colored by time until impact in days.** *The left plot corresponds to a small value of $J_2$ ($J_2$ is half the nominal value), the middle plot is for nominal $J_2$, and the right plot is for a large $J_2$ ($J_2$ is double the nominal value). Larger values of $J_2$ showed fewer impacting trajectories.*

In all impact cases, the impact occurs literally within one hundred days of the start of the orbit propagation. All of the successfully propagating cases safely orbit for twenty years. This behavior can be attributed to the theory of secular perturbation where the argument of perigee and eccentricity evolve over time based on the relative strengths of $J_2$ and $J_3$, as shown below (Ref. 5 - 7)..

$$\frac{d\omega}{dt} = \frac{3nJ_2R^2}{a^2(1-e^2)^2}\left(1-\frac{5}{4}\sin^2 i\right)\left[1+\frac{J_3R}{2J_2a(1-e^2)}\left(\frac{\sin^2 i - e\cos^2 i}{\sin i}\right)\frac{\sin\omega}{e}\right] \tag{3}$$

$$\frac{de}{dt} = -\frac{3nR^3J_3\sin i}{2a^3(1-e^2)^2}\left(1-\frac{5}{4}\sin^2 i\right)\cos\omega \tag{4}$$

For Dawn, the inclination is very close to 90°. It is evident in the equations above that the argument of perigee and eccentricity mutually affect their rate of change over time. Long-term signatures in conic elements can be seen in Figure 3. This figure shows all conic elements for the first nine months of an orbit propagated through a stable combination of $J_2$, $J_3$, and $J_4$ parameters, but still near the boundary of instability (see Figure 1 and 2). Repeating patterns can be seen, and these patterns repeat over much longer propagations of 20+ years. Of interest are the patterns for the argument of periapsis and eccentricity. Argument of periapsis is measured as the angular difference between where the orbit passes through the Ceres equatorial plane and where periapsis occurs. Figure 3 shows that the argument of periapsis is seen to resolve at 180º, progressing to 90º, and then progressing to 0º where it dissolves and resolves again at 180º. During this same time in the orbit, eccentricity begins near 0.0, grows to 0.4 and drops back to 0.0.

The rate of change of the argument of periapsis is described in Equation 3, and this rate is dependent on $J_2$ and $J_3$. The rate of change of the eccentricity is described in Equation 4, and this rate is dependent on $J_3$ and the cosine of the argument of periapsis. This explains the coupling of argument of periapsis and eccentricity: when the argument of periapsis is between 180º and 90º, eccentricity is increasing; when the argument of periapsis is between 90º and 0º, the eccentricity is decreasing.

A closer study of two borderline cases shows the orbital behaviors that differentiate impact and non-impact cases in Figure 2. Figure 4 shows the orbital two elements for the first 100 days of a non-impact case alongside of the orbital elements of an impact case. In both cases, the eccentricity grows from zero to 0.40 over the course of a month (approximately 150 orbits) as the argument of periapsis changes from 180º to 90º. For these and similar cases near the stability boundary, the argument of periapsis "stabilizes" at 90º. After residing at 90º for some time,

if it reverts back above 90º there is a crash as the eccentricity increases further and the periapsis altitude drops below the surface of Ceres. However, if the argument of periapsis continues to advance below 90º and on to 0º, eccentricity drops and the orbit circularizes. The differences in the signatures are highlighted in Figure 4, and are achieved when $J_3$ and $J_4$ are changed by less than 1 part in 10000. Although the non-impacting case propagates safely, it does so with periods of high eccentricity, where the minimum altitude gets down to 20 kilometers. Later sections in this paper will further explain our understanding of the ranges of orbit eccentricity over long periods.

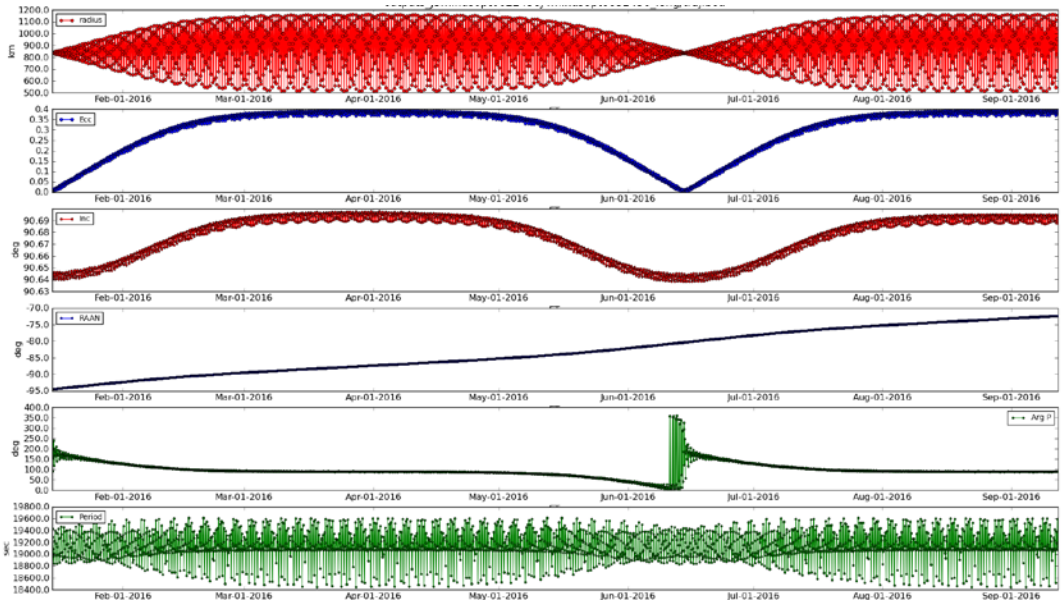


**Figure 3: Cycles in the evolution of a orbital elements for a non-impacting orbit.** *From top to bottom, the plot shows the radius, eccentricity, inclination, right ascension of ascending node, argument of perigee, and period of the orbit. The assumed gravity for this orbit placed it near the impact/non-impact boundary highlighted by Figures 1 and 2.*

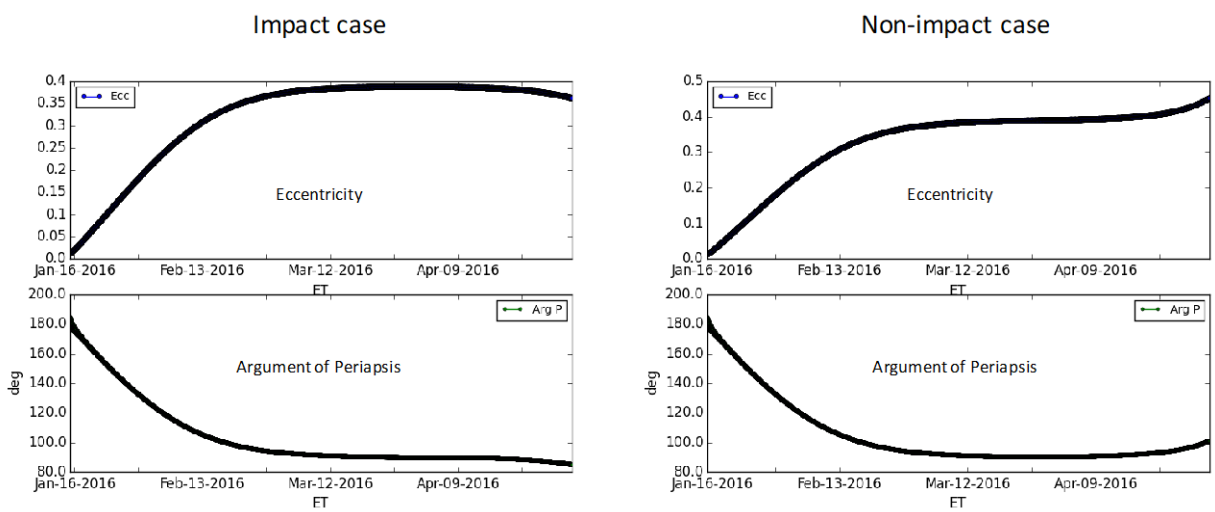


**Figure 4: Comparison of conic element evolution between an impacting orbit and a safe orbit.** *For the non-impact case, $J_3$ = -0.0022430 and $J_4$ = -0.0032430. For the impact case, $J_3$ = -0.0022431 and $J_4$ = -0.0032431.*

## III. Radially Stratified Ceres Gravity Field

The previous section revealed the important interaction between the zonal harmonics. An outstanding question is whether Ceres' zonal harmonics would be such that the LAMO orbit would become unstable over the period of time specified by Planetary Protection. To investigate what gravity field Ceres may have, we set forth on three different

gravitational parameter studies. The first of the gravitational studies aimed to produce a small sample of extreme gravity fields for Ceres. For this approach, we use a code that computes the gravitational coefficients from a density profile and a given topography. This code has been used in other studies. For example, it was used to estimate the moment of inertia for Phobos (Ref. 8) and Mimas (Ref. 9). We call this the direct expansion model for the gravity field which is generated from a heterogeneous density distribution model. The second analysis is based on the Kaula rule (Ref. 10) to size the uncertainty of each spherical harmonics degree. The third analysis is a gravity Monte Carlo study where we generated artificial Ceres gravity fields to yield statistics of each spherical harmonic coefficient. The Kaula rule is theoretical. The first and the third analyses involved construction of gravity fields from available and exaggerated shape models and hypothetical density distributions (Ref. 11), but the assumptions on the internal density distributions used in these models differ. We first discuss the direct expansion model analysis in this section.

The principle of the direct model consists in integrating Ceres elemental volumes in spherical geometry with an assumed profile density and radial law. The discretization is performed by using a unique fundamental angle $\delta$ on the colatitude and longitude. From the constraints on the flattening of Ceres as observed from the earth-based stations and Hubble images (Ref. 3) and the theory of the evolution of a highly flattened celestial body (Ref. 12), Ceres is hypothesized as an icy body that is radially stratified composed of two layers a rocky core of density $\rho_c$ = 2700 kg/m$^3$ and an icy mantle of density $\rho_m$ = 1000 kg/m$^3$ (Ref. 3). Each radial law are decomposed in spherical harmonics, for the surface radius

$$r = r_{mean} \sum_{n=0}^{\infty} \sum_{m=0}^{n} P_{nm}(\sin\phi) \begin{bmatrix} \cos m\lambda \\ \sin m\lambda \end{bmatrix} \cdot \begin{bmatrix} T_{nm} \\ U_{nm} \end{bmatrix} \tag{5}$$

where $T_{nm}$ and $U_{nm}$ are the coefficients of the topography and $r_{mean}$ is taken equal to 476.2 km. The core radius is also expanded in spherical harmonics with coefficients $T_{nm}c$ and $U_{nm}c$.

The surface topography is determined from the measurements from the Hubble images (Ref. 3). They obtained an axi-symetric shape equivalent to an ellipsoid with the equatorial radius equal to 487.3 km and the polar radius equal to 454.7 km. Their uncertainties are 1.8 and 1.6 km, respectively. The topography is then described by a non-zero $T_{20}$ equal to -21.53 km (scaled by $r_{mean}$) and the rest of coefficients equal to zero. The corresponding value for the core is computed by assuming that the interior is at hydrostatic equilibrium (between gravitational and centrifugal accelerations) and $T_{20}c$ is equal to -18.5 km. This axi-symetric model is the nominal model called Ceres-T1 and we develop the other models as perturbation of this model. The second model Ceres-T2 introduces a supplementary $T_{33}c$ equal to 0.3 km and Ceres-T3 explores a higher value for $T_{33}c$ of 0.8 km. The fourth model Ceres-T4 employs a positive $T_{30}$ at the surface of 3.4 km and Ceres-T5 a negative $T_{30}$ value of -3.4 km.

**Table 2. List of topographic anomalies assumed in the reference models and the corresponding normalized gravity coefficients.** *$T_{nm}$ coefficients for the Legendre polynomial, multiplied by the mean radius, describes the global shape. $T_{nm}c$ does the same for the core shape.Only the outstanding values of the spherical harmonics, ~>$10^{-4}$, are highlighted.*

| | CERES-T1 | CERES-T2 | CERES-T3 | CERES-T4 | CERES-T5 |
|---|---|---|---|---|---|
| $T_{20}$ $r_{mean}$ (km) | -21.53 | -21.53 | -21.53 | -21.53 | -21.53 |
| $T_{20}c$ $r_{mean}$ (km) | -18.5 | -18.5 | -18.5 | -18.5 | 18.5 |
| $T_{30}$ $r_{mean}$ (km) | | | | 3.4 | -3.4 |
| $T_{33}c$ $r_{mean}$ (km) | | 0.3 | 0.8 | | |
| $J_2$ | 1.01 x 10-2 | 1.02 x 10-2 | 1.02 x 10-2 | 1.01 x 10-2 | 1.01 x 10-2 |
| $J_3$ | | | | -5.23 x 10-4 | 5.23 x 10-4 |
| $C_{33}$ | | -7.71 x 10-4 | -2.32 x 10-3 | | |
| $J_s$ | -2.39 x 10-4 | -2.41 x 10-4 | -2.60 x 10-4 | -2.41 x 10-4 | -2.41 x 10-4 |

The above direct expansion models are compared with the success/failure criterion of $J_3$ and $J_4$ values for the nominal value of $J_2$ in Figure 5. It is evident that the direct expansion models pose no threat to violating the Planetary Protection guideline. This shows that even the stressed cases that consider topography variation are nowhere close to the success/failure boundary of the long-term orbit propagation.

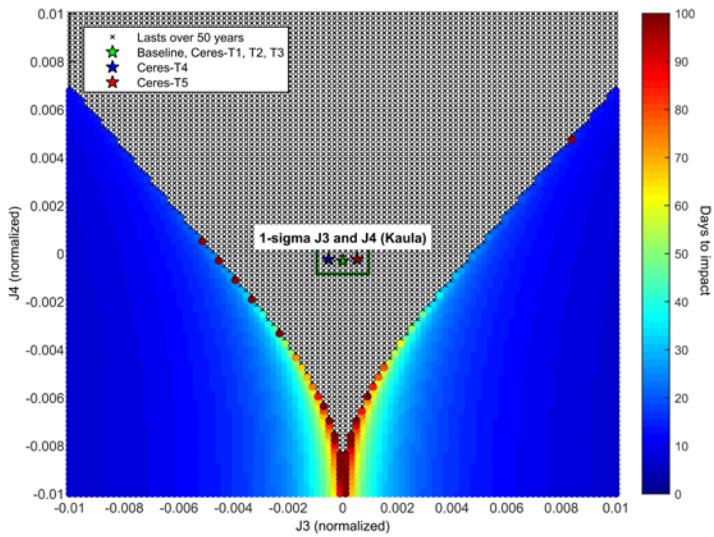


**Figure 5: Success vs failure plot for the nominal $J_2$ with the direct expalnsion models shown as stars.**

## IV. Application of Kaula's Rule and Gravity Monte Carlo Analysis with Two-layer Model

A second study was performed using Kaula's power law as a basis for the variance of the gravity field values. The Kaula's rule is widely used to scale the a priori uncertainty of spherical harmonics. Proposed by Kaula (Ref. 10), that rule has proved to perform well for constraining the uncertainties of the higher-degree terms in the least-square filter for terrestrial planets and other large enough bodies (Ref. 13 and 14). Equations 6 and 7 show how the Ceres Kaula power line is scaled from the Earth's power line based on the mass and the reference radius for the spherical harmonics:

$$\kappa_n = \sqrt{\frac{\sum_{m=0}^{n} C_{nm}^2 + S_{nm}^2}{2n+1}} \approx \frac{K_{Ceres}}{n^2} \tag{6}$$

$$K_{Ceres} = K_{Earth} \left( \frac{M_{Earth}}{M_{Ceres}}^2 \right) \left( \frac{R_{Ceres}}{R_{Earth}} \right)^4 \tag{7}$$

For Ceres, $K_{Ceres}$ is 0.0086. It is important to note that even though the higher-degree terms usually show good agreement with the Kaula power line, the lower-degree terms are usually overly conservative. We will take that into account when sizing the appropriate covariance.

In addition to using Kaula rule as guidance, we also generated Monte Carlo gravity field samples of Ceres based on the two-layer model without assuming constraints on the rotational dynamics (gravity Monte Carlo). The two-layer model is the base model and represents the core and icy shell as ellipsoids. The core radius ranges from 380 – 420 km, and the density from 2.7 to 2.95 g/cm$^3$. The icy shell radius ranges from 480 – 490 km in the x and y axes and 450 – 460 km in the z-axis. Its density is fixed to 1 g/cm$^3$. Since the base model is ellipsoidal, the odd-degree zonals and non-zonal (i.e., tesseral and sectorial) are nominally zero (Ref. 15 and 16).

In addition to the changes in the radii and density values, we also manipulated the topology of the icy shell. For this we used a tool developed by JPL for small body mission analysis (Ref. 17). The tool combines a sinusoidal perturbation modulated by another perturbation distributed as Gaussian. We perturbed the icy shell surface by the maximum amplitude of 12 km (~2-sigma offset based on the observations of Ref. 3) with a wavelength of 100 km and Gaussian perturbation with the maximum amplitude of 5 km for each vertex. The total number of gravity Monte Carlo samples reached 75,000.

**Table 3: The results of the 1-sigma uncertainty of Kaula rule and gravity Monte Carlo for each degree harmonics**. *For each degree term, we compare the magnitude of the 1-sigma covariance by Kaula's rule and gravity Monte Carlo. We found that the gravity Monte Carlo sampling yields significantly smaller 1-sigmas values.*

| Degree | Kaula rule for each degree (1-sigma) | Maximum coefficient uncertainty for each degree from the gravity MC (1-sigma) |
|---|---|---|
| 2 | 2e-3 | 1e-3 |
| 3 | 1e-3 | 8e-4 |
| 4 | 5e-4 | 1.5e-4 |
| 5 | 3e-4 | 1e-4 |
| 6 | 2e-4 | 1e-4 |

The resulting statistics are shown in Table 3. The gravity Monte Carlo yields smaller uncertainties than the Kaula rule. This result indicates that it is challenging to perturb the Ceres' gravity field while comforming to assumptions of the two-layer model. Also note that the uncertainties used for the orbital MC (Table 1) are significantly larger than those in Table 3 except for $J_2$. That is, the uncertainties used for the orbital MC are more conservative than the Kaula rule or the gravity MC. When the 1-sigma uncertainty from Table 1 is used to seed an orbital propagation MC study in Section II, some of the samples result in $J_3$ and $J_4$ values that lead to crashes (Figure 1). Even though some samples lead to impacting, they were drawn from a more conservative pool of statistics than predicted by either Kaula or the gravity MC. Furthermore, some parameters that were used for orbital MC analysis far exceeded the expected range of possible values that were not even realized by the stressed cases of the direct expansion models. Thus, it was concluded that the trajectories that survived a long-term propagation included those that are both physical and aphysical (or in other words, highly non-hydrostatic). Therefore, the analysis discussed here is conservative.

## V. Gravity Monte Carlo with Best-effort, Pre-arrival Gravity Model

Based on all the above analyses, a current-best-estimate (CBE) gravity field covariance was created for the planetary protection lifetime analyses. Members of the Navigation and Science Teams went one-by-one through each spherical harmonic coefficient and decided on conservative mean and 1σ values. Off diagonal terms were set to zero to be conservative since sampling such a covariance sometimes results in more challenging, i.e. non-plausible, gravity fields than if cross correlations were supplied. The CBE covariance values are listed in Table 4 and was the covariance used in the lifetime analysis presented in this report.

**Table 4: The final agreed-upon mean and covariance for the 6x6 gravity field used for the orbital MC analysis.** *The mean and covariance values were carefully chosen from the Monte Carlo Ceres gravity field population. This input gravity field resulted in zero crashing event over 50 years for 10,000 samples.*

| Coefficient | Baseline | CBE | |
|---|---|---|---|
| | | Mean | 1σ |
| $J_2$ | 9.40E-03 | 9.00E-03 | 1.00E-03 |
| $J_3$ | 0 | 0 | 3.00E-04 |
| $J_4$ | -3.16E-04 | -3.20E-04 | 1.50E-04 |
| $J_5$ | 0 | 0 | 1.00E-04 |
| $J_6$ | 3.05E-05 | 3.00E-05 | 1.00E-04 |
| $C_{21}$ | 0 | 0 | 1.00E-03 |
| $S_{21}$ | 0 | 0 | 1.00E-03 |
| $C_{22}$ | 0 | 0 | 1.00E-03 |
| $S_{22}$ | 0 | 0 | 1.00E-03 |
| $C_{31}$ | 0 | 0 | 3.00E-04 |
| $S_{31}$ | 0 | 0 | 3.00E-04 |
| $C_{32}$ | 0 | 0 | 3.00E-04 |
| $S_{32}$ | 0 | 0 | 3.00E-04 |
| $C_{33}$ | 0 | 0 | 8.00E-04 |
| $S_{33}$ | 0 | 0 | 3.00E-04 |
| $C_{41}$ | 0 | 0 | 1.00E-04 |
| $S_{41}$ | 0 | 0 | 1.00E-04 |
| $C_{42}$ | 0 | 0 | 1.00E-04 |
| $S_{42}$ | 0 | 0 | 1.00E-04 |
| $C_{43}$ | 0 | 0 | 1.00E-04 |
| $S_{43}$ | 0 | 0 | 1.00E-04 |
| $C_{44}$ | 0 | 0 | 1.00E-04 |
| $S_{44}$ | 0 | 0 | 1.00E-04 |
| $C_{51}$ | 0 | 0 | 1.00E-04 |
| $S_{51}$ | 0 | 0 | 1.00E-04 |
| $C_{52}$ | 0 | 0 | 1.00E-04 |
| $S_{52}$ | 0 | 0 | 1.00E-04 |
| $C_{53}$ | 0 | 0 | 1.00E-04 |
| $S_{53}$ | 0 | 0 | 1.00E-04 |
| $C_{54}$ | 0 | 0 | 1.00E-04 |
| $S_{54}$ | 0 | 0 | 1.00E-04 |
| $C_{55}$ | 0 | 0 | 1.00E-04 |
| $S_{55}$ | 0 | 0 | 1.00E-04 |

Using the covariance values in Table 4, a CBE Monte Carlo analysis was performed for 10,000 samples. Figure 6 shows a histogram of the minimum radius encountered during each 50 year propagation for the Monte Carlo analysis. We chose the 50-year propagation to be conservative.

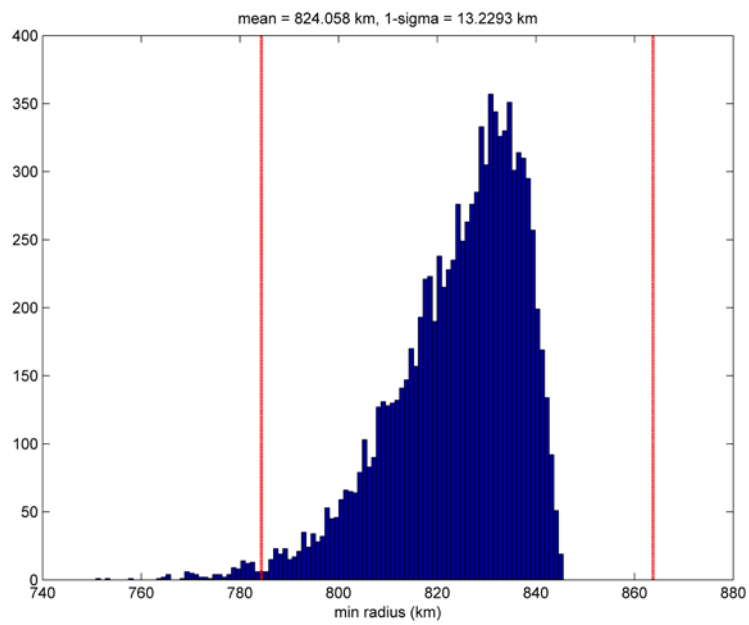


**Figure 6: Histogram of the minimum orbit radius for 10,000 orbits propagated through 10,000 Ceres Gravity fields with ±3σ lines in red.** *Impact is expected to only occur below 480 km (thus, no impacts were detected).*

The 3σ low of the minimum radius (left red vertical line) encountered amongst all cases was 784 km which is more than 300 km in altitude. Therefore, none of the 10,000 Monte Carlo cases came anywhere close to impacting Ceres. This final CBE orbit MC study showed that, for the statistics given in Table 4, Dawn will be safely placed in LAMO with no risk of impacting to the surface.

## VI. Gravity Model with Updated Shape Model

The Dawn spacecraft began imaging Ceres starting in January 2015. By late January 2015, the spatial resolution exceeded the Hubble images. This allowed the Optical Navigation team to construct a new Ceres shape model, which was used for another iteration of gravity MC analysis in March 2015. We refer to it as the 2015 gravity MC analysis. Since the topography is fixed to the Opnav shape model, we did not need to manipulate the surface topology as previously done. This reduced the total sample size to roughly 1600. The following Figures 7(a) through (c) show the comparison of each spherical harmonic coefficient between the CBE gravity in Section V and the 2015 gravity MC analysis. The blue error bars denote the CBE gravity and the red ones the 2015 gravity MC analysis using the updated shape model. At that time the Dawn spacecraft was in Survey and was too far from the dwarf planet to sense $J_3$ and $J_4$ with sufficient accuracy. $J_2$ was estimated to be 7.6e-3 ± 9e-4 which is well within the bounds of the 2015 gravity MC analysis.

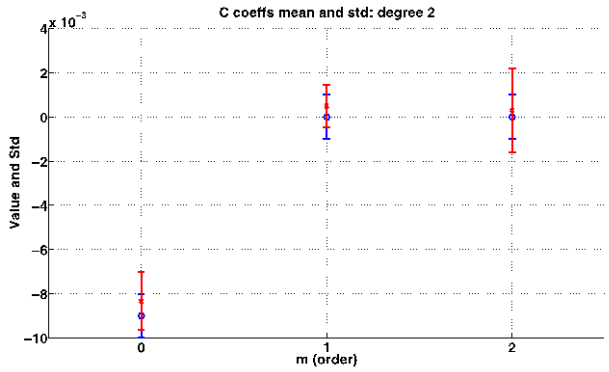


Figure 7 (a): Second-degree harmonics.

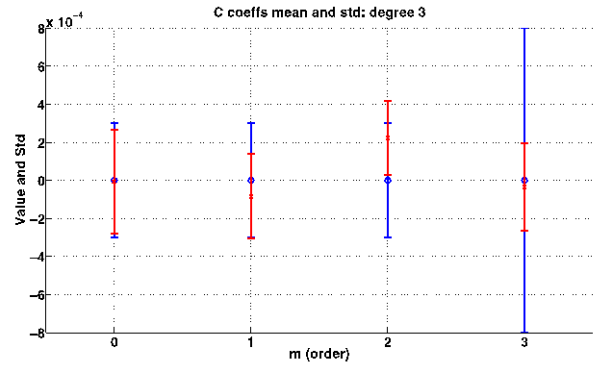


Figure (b): Third-degree harmonics.

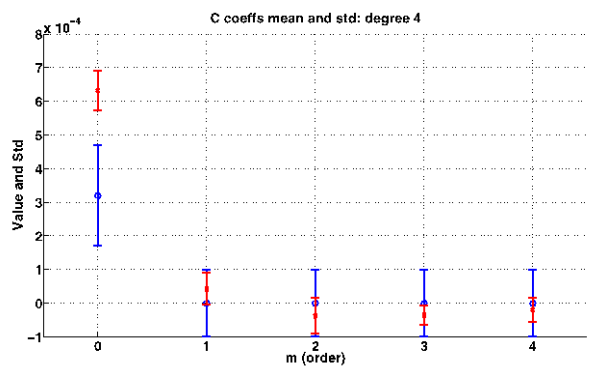


Figure 7 (c): Fourth-degree harmonics.

**Figure 7: The values and 1-sigma uncertainty of the second, third, and fourth degree harmonics for the CBE gravity analysis (blue) and 2015 gravity MC analysis (red).** *Note that the values are for the C zonal harmonics, so its sign is the opposite of the J zonal harmonics. Assuming three-sigma, the blue and red error bars overlap.*

By observing the figures above, both $J_2$ and $J_3$ share similar values for the CBE gravity and 2015 gravity MC analysis. The $J_4$ mean values differ by more than 1-sigma of each respective uncertainty, but basing on a larger uncertainty of the CBE gravity analysis, the $J_4$ statistics for the 2015 gravity MC analysis agrees within the 2-sigma level. This result reassured that the new shape model did not alter the results of the pre-arrival planetary protection analysis.

## VII. Comparison of the MC Gravity Field with respect to the HAMO Estimated Gravity Field

In this section, we compare the CBE orbital MC analysis (Section V) against that estimated from the HAMO dataset. The HAMO gravity field is used because it represents the best estimate of the gravity field before Dawn's orbit was lowered to LAMO where the orbital stability is paramount. Table 5 reports the values and 1-sigma uncertainties for $J_2$ through $J_4$ estimated by Ref. 18.

*Table 5: Best estimate of $J_2 - J_4$ from the HAMO data (radio + optical)*

| | Value | 1-sigma uncertainty |
|---|---|---|
| $J_2$ | 1.1506e-2 | 1e-6 |
| $J_3$ | -4.96e-5 | 1.4e-6 |
| $J_4$ | -5.25e-4 | 3e-6 |

The above table shows that the HAMO-estimated zonal harmonics sit within the statistics presented in Table 4. Thus, the Dawn spacecraft is not at risk of impacting the surface of Ceres after its disposal in LAMO.

## VIII. Conclusion

Prior to Dawn's arrival at Ceres in 2015, the planning of the nominal mission required that Dawn's final orbit would not impact the surface of Ceres over a period of 20 years. This requirement was stipulated by Planetary Protection, and the Dawn navigation team was tasked with substantiating that the lowest science orbit would not pose a threat to this requirement. First, the sensitivity of spherical harmonics to the long-term dynamical propagation was investigated. This preliminary analysis showed strong correlations between the $J_2$, $J_3$, and $J_4$ coefficients to the orbit stability in LAMO. The stable orbits exist in the valley of $J_3$ and $J_4$ diagram, and the larger $J_2$ value increases the stability region. Second, heterogeneous density distribution models that conform to the constraints by Ceres' rotational dynamics of Ceres were constructed, assuming a two-layer interior. These models yield the point solutions that push the possible boundary of the harmonic values. However, none of them threatened the orbital stability in LAMO.

We further refined our investigation by performing a more statistical approach to the gravity field sampling. To this end we constructed a two-layer model (core and icy shell) that meets the limitations set forth by the Ceres' dimensions and hydrostatic equilibrium. The variables are the density values for each layer and their dimensions. The result is the mean and 1-sigma uncertainty of each spherical harmonic coefficient. These numbers together with the Kaula rule gave a guideline on the statistical distribution of the Ceres gravity field, and the orbital Monte Carlo was rerun to find a small number of samples crashing into the surface. All the failure cases have been determined to be unreasonable after we verified that even the most extreme topography and density variations cannot produce such gravity fields. Thus this pre-arrival planetary protection analysis validated that the final nominal LAMO would be a safe disposal orbit.

Dawn arrived at Ceres in March 2015. After the initial acquisition of the optical images, a more accurate Ceres shape model became available. Then, using the observed shape to better constrain the topology, the same gravity Monte Carlo analysis was repeated in order to ensure that the nominal plan still remained compliant with the planetary protection requirement. This was validated, and we further confirmed with the HAMO data that the planetary protection is still honored. As of August 2016, the Dawn spacecraft is in the extended mission phase.

## Acknowledgments

This work was supported by the NASA Dawn project and conducted at the Jet Propulsion Laboratory, California Institute of Technology under a contract with NASA. Copyright 2016. All rights reserved. Rambaux acknowledges funding from the French National Programme of Planetology (PNP) and code comparisons as well as fruitful discussions with B. Gaskell.

## References

[1]Russell, C. T., Raymond, C. A., The Dawn Mission to Vesta and Ceres, Space Science Reviews, 2011, Volume 163, Issue 1-4, pp. 3-23.

[2]NASA Procedural Requirements 8020.12D, Planetary Protection Provisions for Robotic Extraterrestrial Missions, http://nodis3.gsfc.nasa.gov/npg_img/N_PR_8020_012D_/N_PR_8020_012D_.pdf

[3]Thomas, P. C., Parker, J. W., McFadden, L. A., Russell, C.T., Stern S.A., Sykes M.V., Young E.F., Differentiation of the Asteroid Ceres as Revealed by its Shape. Nature 437, 224–226 (2005).

[4]Baer, J., Chesley, S.R., Matson, R.D., 2011. Astrometric masses of 26 asteroids and observations on asteroid porosity. Astronomical Journal. 141, 143, 12pp

[5]Cook, R., The Long-term Behavior of Near-circular Orbits in a Zonal Gravity Field, AAS/AIAA Astrodynamics Specialist Conference, AAS paper 91-463, Durango, Colorado, 1991.

[6]Cutting, E., Frautnick, J. C., Born, G. H., Pardal, P., Orbit Analysis for Seasat-A, Journal of the Astronautical Sciences, vol. 26, Oct.-Dec. 1978, p. 315-342.

[7]Pardal, P., Kuga, H., Moraes, R., Study of Orbital Elements on the Neighbourhood of a Frozen Orbit, Journal of Aerospace Engineering, Sciences and Applications, May – Aug. 2008, Vol. I, No 2.

[8]Rambaux, N., Castillo-Rogez, J.C., Le Maistre, S., & Rosenblatt, P., 2012, Rotational motion of Phobos, Astronomy and Astrophysics, Vol 548, id.A14, 11pp.

[9]Tajeddine R., Rambaux, N., Lainey, V., Charnoz, S., Richard, A., Rivoldini, A., Noyelles, B., 'Mimas' surprising interior: Strong constraints from Cassini ISS libration measurements', Science, Volume 346, Issue 6207, pp. 322-324 (2014)

[10]Kaula, W. M., Theory of Satellite Geodesy, Blaisdell, Waltham, MA, 1966, pp. 92–107, Chap. 5.

[11]Werner, R. A., Spherical Harmonic Coefficients for the Potential of a Constant-Density Polyhedron, Computers and Geosciences, Vol. 23, No. 10, 1997, pp. 1071–1077.

[12]Rambaux, N., Chambat, F., Castillo-Rogez, J.C., Third-order Development of Shape, Gravity, and Moment of Inertia for Highly Flattened Celestial Bodies. Application to Ceres., Astronomy & Astrophysics, Volume 584, id.A127, 8pp.

[13]Konopliv, A.S., Asmar, S.W., Park, R.S., Bills, B.G., Centinello, F., Chamberlin, A.B., Ermakov, A., Gaskell, R.W., Rambaux, N., Raymond, C.A., Russell, C.T., Smith, D.E., Tricarico, P., Zuber, M.T., The Vesta Gravity Field, Spin Pole and Rotation Period, Landmark Positions, and Ephemeris from the Dawn Tracking and Optical Data, Icarus, 2014, 240, 103 – 117.

[14]Lemoine, F.G., Goossens, S.J., Sabaka, T.J., Nicolas, J.B., Mazarico, E., Rowlands, D.D., Loomis, B.D., Chinn, D.S., Caprette, D., Neumann, G.A., Smith, D.E., Zuber, M.T., Modeling and Precise Orbit Determination in Support of Gravity Model Development for the Grail Mission, AAS/AIAA Space Flight Mechanics Meeting, AAS Paper 13-273, Kauai, Hawaii, 2013.

[15]McCord, T. B. and Sotin, C., Ceres: Evolution and Current State. Geophys. Res. Lett. 110, E05009 (2005).

[16]Castillo-Rogez, J.C., McCord, T.B., Ceres' Evolution and Present State Constrained by Shape Data, Icarus, 2010, 250, 443 - 459.

[17]Broschart, S.B., Abrahamson, M., Bhaskaran, S., Fahnestock, E.G., Karimi R.R., Lantoine G., Pavlak, T.A., Chappaz, L., The Small-Body Dynamics Toolkit and Associated Close-Proximity Navigation Analysis Tools at JPL, AAS Guidance and Control Conference, Breckenridge, CO, Jan. 30 – Feb. 4, 2015. AAS 15-127.

[18]Kennedy, B. M., Bradley, N.E., Han, D., Karimi, R.R., Mastrodemos, N., Rush, B., Takahashi, Y., Determination of Ceres Physical Parameters Using Radiometric and Optical Data, 2016 AAS GN&C Conference, AAS Paper 16-107, Breckenridge, CO, 2016